Spatiotemporal pattern formation in counterpropagating two-wave mixing with an externally applied field

O. Sandfuchs and F. Kaiser

Institute of Applied Physics, Darmstadt University of Technology, Hochschulstrasse 4a, 64289 Darmstadt, Germany

M. R. Belić

Institute of Physics, P.O. Box 57, 11001 Belgrade, Yugoslavia

The spatiotemporal dynamics of two counterpropagating beams in a photorefractive crystal with nonlocal and sluggish response is investigated in the longitudinal and one transverse dimension. A static external electric field is applied to the crystal to control the coupling strength of the two-wave mixing process. A nonautonomous linear stability analysis is performed that takes a nonconstant modulation depth into account. The onset of pattern formation for arbitrary coupling constants and pump ratios and the influence of linear absorption are discussed. Above the threshold predicted by stability analysis, running transverse waves appear in the optical near field and wandering spots appear in the corresponding far field. A nonlinear eigenmode analysis reveals the running transverse waves as secondary instabilities. © 1998 Optical Society of America [S0740-3224(98)00407-X]

OCIS codes: 190.4420, 190.5330, 190.7070.

1. INTRODUCTION

Spatiotemporal pattern formation through two counterpropagating optical beams in a nonlinear medium has been observed experimentally and investigated theoretically in a variety of systems: Kerr media,[1–4] atomic vapors,[5] and Brillouin scattering.[6] The pump beams became unstable against the formation of sideband beams, which were observed in the optical far field as spots or arrays of spots.

In recent years transverse instabilities and transverse pattern formation have also attracted considerable interest in the field of photorefractive (PR) media. First experiments were performed with a feedback mirror,[7–9] and rotating hexagonal spots in the far field were observed. Honda and Banerjee were able to give a theoretical explanation of their measurements.[10] They emphasized that though hexagonal patterns are formed through reflection gratings of the pump beams, transmission gratings between pump beams and their own sideband beams are of importance.

Some PR crystals, e.g., LiNbO$_3$, exhibit no phase shift between the intensity variation and the variation in the refractive index. The onset of pattern formation owing to this local medium response was thoroughly studied by Sturman and Chernykh.[11,12] Saffman *et al.*[13,14] considered both the local and the nonlocal responses of PR media. The nonlocal response occurs for BaTiO$_3$ and KNbO$_3$, for example, and leads to an energy exchange between the pump beams. Thus one has to deal with a nonautonomous stability problem when predicting the onset of pattern formation in these types of PR crystal. Saffman *et al.* considered interaction through both transmis-

sion and reflection gratings but in the latter case considered only constant internal pump ratio to obtain an analytical threshold condition.

Theoretical investigations with nonlocal PR response are impeded by the fact that transverse structures occur through reflection gratings, a situation that is known to cause great difficulties for both analytical and numerical treatment. Theoretical predictions by means of linear stability analyses[10,14] offered improved understanding of the origin of the structures but could not reveal the spatiotemporal dynamics that occurs above the primary instability threshold.

In this paper we present theoretical and numerical investigations of spatiotemporal structures that are due to counterpropagation of two pump beams in a PR crystal with nonlocal and sluggish medium response by interaction through reflection gratings. Extending the previous research, we perform linear stability analysis for the nonautonomous system that results from the inclusion of nonconstant modulation depth.

2. MODEL EQUATIONS

The two-wave mixing process is described by the propagation of two beams through a nonlinear PR medium and their interaction with the medium. Below we consider the standard PR two-wave mixing equations in paraxial approximation of the form[15,16]

$$\partial_z A_1 + if\partial_x{}^2 A_1 + \alpha A_1 = -QA_2, \tag{1a}$$

$$-\partial_z A_2 + if\partial_x{}^2 A_2 + \alpha A_2 = Q^*A_1. \tag{1b}$$

$A_{1,2}(x, z)$ are the slowly varying envelopes of the beams, $f = L/(2k_0 w_0^2)$ is a measure of the magnitude of diffraction and is proportional to the inverse Fresnel number, where L is the length of the crystal, and k_0 denotes the wave vector within the crystal in the longitudinal direction z. Transverse coordinate x is scaled to beam radius w_0. We consider only one transverse dimension. Parameter α is the coefficient of linear absorption. The temporal evolution of the complex amplitude Q of the reflection grating in the crystal is approximated by a relaxation equation of the form[17]

$$\tau \partial_t Q + \eta Q = \Gamma \frac{A_1 A_2{}^*}{|A_1|^2 + |A_2|^2}, \qquad (2)$$

where τ is the relaxation-time constant of the grating describing the sluggish behavior of PR media, η is a parameter that depends on the internal electric fields of the crystal, and Γ is the PR coupling constant. To be able to control the coupling strength of the crystal we apply a static external electric field $E_0 = V/L$ to the crystal in the direction of the grating wave vector. In this case we have, according to Kukhtarev *et al.*,[17]

$$\eta = \frac{E_d + E_q + iE_0}{E_M + E_d + iE_0}, \qquad (3)$$

$$\Gamma = \Gamma_0 \left(1 + \frac{E_q}{E_d} \right) \frac{E_d + iE_0}{E_M + E_d + iE_0}, \qquad (4)$$

with Γ_0 being the steady-state coupling strength without external field. $E_d = 1$ kV/cm, $E_q = 5$ kV/cm, and $E_M = 100$ kV/cm are the values of the internal fields that describe the electronic processes in a $BaTiO_3$ crystal.[18] Note that E_0 effectively renders both coupling constant Γ and relaxation-time constant τ complex. Hence E_0 exerts a profound influence on the process of wave mixing. By breaking the frequency degeneracy it allows for the buildup of running gratings and the appearance of running transverse waves.

All explicit spatial dependences in Q are neglected. As a consequence the temporal evolution in Eq. (2) is adiabatically separated from the spatial variations in Eqs. (1). In reflection geometry we are dealing with two-point boundary conditions at the opposite faces of the crystal (Fig. 1). Boundary conditions are chosen consistently with the common experimental conditions to be Gaussian beams in combination with open lateral sides (no reflecting or periodic boundaries):

$$A_1(x, z = 0) = C_1 \exp(-x^2/w_0^2),$$

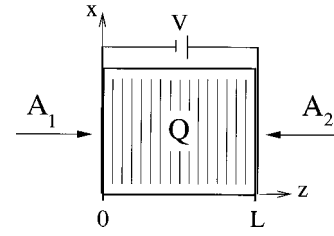$$A_2(x, z = L) = C_2 \exp(-x^2/w_0^2). \qquad (5)$$

Fig. 1. Two-wave mixing configuration in reflection geometry with an externally applied voltage V: A_1, A_2, pump beams; Q, grating amplitude. z indicates the direction of propagation, and x is the transverse dimension.

Inasmuch as only the input intensity ratio $r_0 = I_1(0)/I_2(L)$ of the beams is a relevant parameter, we can put $C_1 = 1.0$ and $C_2 = r_0^{-1/2}$.

3. LINEAR STABILITY OF TRANSVERSE MODES

The primary instability threshold for the onset of transverse patterns is determined by the linear instability of the steady-state plane-wave solutions. These steady-state plane-wave solutions ($f = 0$ and $\partial_t Q = 0$) without absorption were derived by Yeh[19]; those including absorption, by Belić.[20] They are the spatially homogeneous fixed-point solutions of the system.

The steady-state field amplitudes are denoted by $A_1^0(z)$ and $A_2^0(z)$, and the corresponding amplitude of the refractive-index grating is denoted by $Q^0(z)$. The stability analysis proceeds with a small perturbation of the wave and grating amplitudes:

$$A_1(z, x, t) = A_1^0(z)[1 + \epsilon a(z, x, t)], \qquad (6a)$$

$$A_2(z, x, t) = A_2^0(z)[1 + \epsilon b(z, x, t)], \qquad (6b)$$

$$Q(z, x, t) = Q^0(z)[1 + \epsilon q(z, x, t)]. \qquad (6c)$$

After Eqs. (6) are substituted into Eqs. (1) and (2) the perturbations a, b, and q will be expanded in the transverse Fourier ($x \rightarrow K$) and in the temporal Laplace ($t \rightarrow \lambda$) space, yielding an algebraic expression for q. After elimination of q, the linearized equations are cast into a matrix form:

$$\partial_z \mathbf{a} = \mathcal{A}(z, K, \lambda) \mathbf{a}(z, K, \lambda). \qquad (7)$$

The vector $\mathbf{a} = (a_+, a_-, b_+, b_-)^T$ contains the Fourier–Laplace components of the perturbations, where $a_\pm$ and $b_\pm$ pertain to $\pm|K|$. When we choose an appropriate basis through a transformation $\mathcal{U}$, the physics that is involved in linear stability analysis becomes more obvious. The perturbation matrix reads as

$$\mathcal{A} = \mathcal{U}^{-1} \begin{bmatrix} m_0^2 \gamma + (1 - m_0^2)g(\lambda) & -fK^2 & 0 & -s\sqrt{1 - m_0^2}h(\lambda) \\ m_0^2 \beta + (1 - m_0^2)h(\lambda) + fK^2 & 0 & 0 & s\sqrt{1 - m_0^2}g(\lambda) \\ s\sqrt{1 - m_0^2}g(\lambda) & 0 & 0 & -h(\lambda) - fK^2 \\ s\sqrt{1 - m_0^2}h(\lambda) & 0 & fK^2 & g(\lambda) \end{bmatrix} \mathcal{U}. \qquad (8)$$

The temporal variations in Q that are due to the sluggish PR response, which enter through $q(\lambda)$, result in the two functions

$$g(\lambda) = \frac{\lambda}{2}\left(\frac{\Gamma_e \tau_e}{\lambda \tau_e + 1} + \frac{\Gamma_e^* \tau_e^*}{\lambda \tau_e^* + 1}\right), \qquad (9)$$

$$h(\lambda) = \frac{\lambda}{2i}\left(\frac{\Gamma_e \tau_e}{\lambda \tau_e + 1} - \frac{\Gamma_e^* \tau_e^*}{\lambda \tau_e^* + 1}\right). \qquad (10)$$

γ and β are the real and the imaginary parts of the effective coupling constant $\Gamma_e = \Gamma/\eta$; they correspond to the intensity and phase coupling constants, respectively. $\tau_e = \tau/\eta$ is the effective complex PR time constant, and $s = \text{sign}[I_1^0(z) - I_1^0(z)]$.

We can see from this form of stability matrix that the steady-state fixed-point solution contributes only through its modulation depth:

$$m_0(z) = \frac{2[I_1^0(z)I_2^0(z)]^{1/2}}{I_1^0(z) + I_2^0(z)} \qquad (11)$$

to stability. Moreover, linear absorption affects stability only through changes in the modulation depth dependence of the steady-state fixed point and does not occur in $\mathcal{A}$ explicitly.

Owing to energy exchange and linear absorption, nonautonomous equation (7) cannot in general be solved analytically. Nonetheless, its formal solution is given by $\mathbf{a}(L) = \mathcal{F}(L)\mathbf{a}(0)$, where $\mathcal{F}(z)$ is the linear flow matrix. Hence the problem of linear stability is solved if $\mathcal{F}(L)$ is known. Separating $\mathcal{A}$ into $\text{Tr}\,\mathcal{A}$ and its trace-free part, we can calculate $\mathcal{F}(L)$ from

$$\mathcal{F}(L) = \exp\left[\int_0^L \text{Tr}\,\mathcal{A}(s)\mathrm{d}s\right] \times \prod_{z=0}^{L} \mathcal{D}(z). \qquad (12)$$
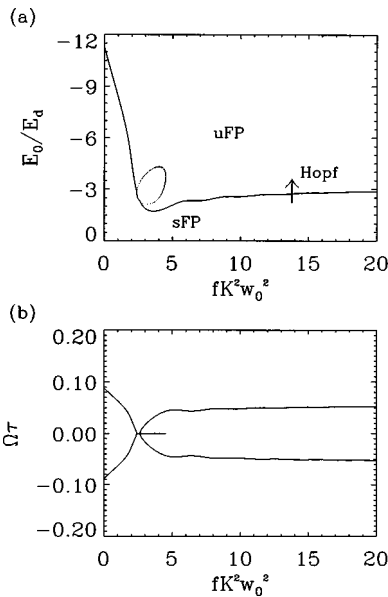

(a)

(b)

Fig. 2. (a) Threshold curves of the applied electric field and (b) threshold frequency of the grating amplitude, as functions of the transverse wave vector K. The coupling constant is $\Gamma_0 L = 2.0$, and the pump ratio $r_0 = 20.09$. sFP, uFP, regions of stable and unstable fixed points, respectively; Hopf, the type of bifurcation as the threshold curve is crossed in the direction of the arrow.

The trace-free part is obtained through a repeated multiplication of infinitesimal rotation matrices $\mathcal{D}(z)$ taken at subsequent points z in the crystal. These matrix products have to be evaluated numerically.

Taking into account two-point boundary conditions, we convert $\mathcal{F}(L)$ into a scattering matrix $\mathcal{S}$ and obtain the final form of the solution:

$$\mathbf{a}(z_{\text{out}}) = \mathcal{S}(K, \lambda)\mathbf{a}(z_{\text{in}}), \qquad (13)$$

where z_{out} and z_{in} denote the output and the input faces of the crystal for the respective beams. The poles of the scattering matrix determine the properties of an absolute instability and lead to the threshold condition.

Under the special constraint for the input intensity ratio r_0, $\ln r_0 = \gamma L$, which implies a ratio of beam intensities inside the crystal $r(z) = I_1^0(z)/I_2^0(z) \equiv 1$ and a modulation depth $m_0(z) \equiv 1$, Eq. (12) reduces to $\mathcal{F}(L) = \exp(\mathcal{A}L)$. Then we obtain the well-known analytical expression for the threshold condition[21]:

$$\cosh\left(\frac{\gamma - g}{2}\right) + \cos(\chi_1)\cos(\chi_2) + p\,\text{sinc}(\chi_1)\text{sinc}(\chi_2) = 0, \qquad (14)$$

where $\chi_1^2 = fK^2(fK^2 + \beta) - \gamma^2/4$, $\chi_2^2(\lambda) = fK^2(fK^2 + h) - g^2/4$, and $p(\lambda) = fK^2[fK^2 + (\beta + h)/2)] + \beta h/2 + \gamma g/4$.

The stability analysis of a spatially extended system results in growth rates $\sigma = \Re(\lambda)$ for the transverse modes K together with their oscillation frequencies $\Omega = \Im(\lambda)$. The instability threshold is inferred from the lowest-lying branches of the stability condition of the most unstable mode: $\sigma_{\max}(K; \Gamma_0, E_0, r_0) = 0$. The polarity of the external field exerts a profound influence on the stability behavior of the medium. In the case of positive polarity ($E_0 > 0$) the threshold condition yields the so-called high-K instability.[21] In our numerical simulations there is an indication that high-K instabilities indeed exist.

In the case of $E_0 < 0$ the instability curves are displayed in Fig. 2 for a constant input pump ratio r_0 without any constraint on internal pump ratios $r(z)$, as in Ref. 21. As long as $|E_0|$ is smaller than a critical value, there is a region of stability for any transverse mode. At a critical value $E_0^c \approx -1.7E_d$ a finite band of transverse modes around a critical mode $fK_c^2 \approx 3.6w_0^{-2}$ is predicted to become unstable through a Hopf bifurcation with a characteristic oscillation frequency $\Omega_c \tau \approx 0.031$. The region where the balloon is displayed corresponds to a static instability. Its threshold, though, is always higher than that of the dynamic instability and therefore is not observable. In addition, the slow medium response leads to plane-wave instabilities ($fK^2 = 0$) whose threshold is much higher ($E_0^c \approx -11.3E_d$) than that for the modal instability.

The solution of the nonautonomous stability problem enables us to discuss the onset of pattern formation for arbitrary parameter values of coupling strength Γ_0 and input pump ratio r_0. In Fig. 3 the primary instability threshold is displayed as a function of coupling strength Γ_0. The threshold value of E_0 becomes the lowest for high Γ_0. The minimum threshold, in the sense that both
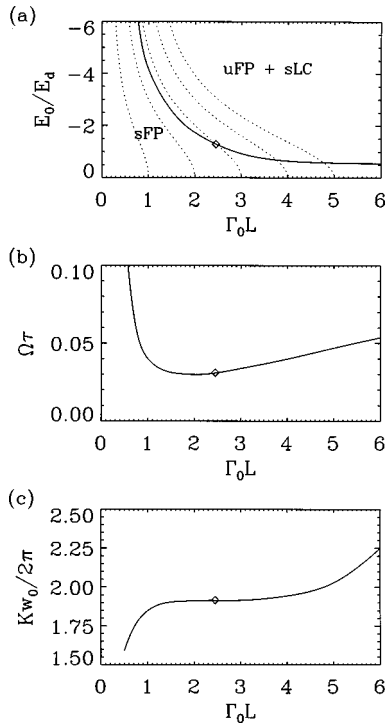
Fig. 3. (a) Bifurcation diagram of the primary instability threshold (solid curve), displaying the critical values of $E_0 < 0$ as a function of $\Gamma_0 L$ for fixed $r_0 = 20.09$. Dashed curve, constant values of the intensity coupling strength $\gamma L = 1.0, 2.0, 3.0, 4.0, 5.0$ (left to right); sFP, and uFP+sLC, regions of stable and unstable fixed points and stable limit cycle, respectively. (b) Oscillation frequency, (c) spatial frequency. Diamonds, points where the threshold values can be obtained analytically.
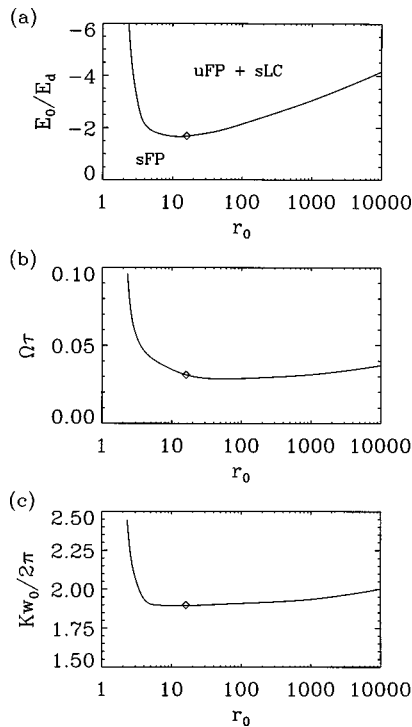

Fig. 4. (a) Bifurcation diagram of the primary instability threshold, displaying the critical values of $E_0 < 0$ as a function of r_0 for fixed $\Gamma_0 L = 2.0$. (b) Oscillation frequency, (c) spatial frequency. Diamonds, points where the threshold values can be obtained analytically.

$E_0{}^c$ and $\Gamma_0{}^c$ simultaneously reach a minimum value, which is the case when the threshold curve in Fig. 3(a) has slope -1, is attained for $\Gamma_0 L \approx 2.4$ and indeed coincides with the maximal value of the modulation depth, in accordance with the presumption in Ref. 14. The critical value of E_0 increases for small coupling strengths. For $\Gamma_0 L < 0.4$ the fixed point is stable for any applied field strength. Figure 4 displays the dependence of the instability threshold on the pump ratio. Here, for a constant value of Γ_0, the threshold again reaches its minimum for that value of r_0 for which the modulation depth attains its maximum value of 1. For equal pump intensities the fixed point is stable for any applied field strength.

The type of bifurcation remains the same, regardless of whether we assume a z-dependent modulation depth. We always find a dynamic instability through a Hopf bifurcation. An applied field always forms a running grating, which, together with the light fields, displays self-sustained oscillations above threshold. We do not find instabilities of this type without an externally applied field.

4. SPATIOTEMPORAL DYNAMICS

For a negative polarity of E_0 our linear stability analysis predicts the spontaneous destabilization of the homogeneous fixed-point solution above a primary threshold value of the applied electric field. To see which spatiotemporal structures arise, we investigate the counterpropagating two-wave mixing process by numerical simulations of the full set of coupled nonlinear wave equations (1) and (2). We use the modified beam propagation method,[15] which we have extended to reflection gratings by means of a relaxation method, to satisfy the two-point boundary conditions. In this and the subsequent sections we keep the following parameters constant:

$$\Gamma_0 L = 2.0, \qquad r_0 = 20.09, \qquad f = 0.025.$$

The strength of external field E_0 is our bifurcation parameter.

In our numerical simulations we find the threshold field strength to be somewhat higher ($E_0{}^c \approx -1.9 E_d$) than predicted ($E_0{}^c \approx -1.7 E_d$), because the transverse modes were considered to be infinitely extended when the stability analysis was performed, whereas we deal with finite Gaussian beam profiles in our simulations. This difference may lead to discrepancies, but the approximation is good as long as the wavelength of modulation remains small enough compared with the beam waist. In Fig. 5 the transverse intensity and phase profiles of the backward-propagating beam at the output face of the crystal are shown at two subsequent times that are half an oscillation cycle apart, when the beam center goes through either its maximal or its minimal intensity.

Below threshold [Figs. 5(a) and 5(c)] we find the fixed point to be an attractor with a smooth Gaussian beam profile. The phase is curved to the edges of the transverse profile, indicating the self-focusing behavior as a consequence of the Gaussian beam shape in the intensity. Slightly above threshold [Figs. 5(b) and 5(d)] a spontaneous modulation of the beam profile and the phase distribution appears. This modulation oscillates in time, and

we find a limit cycle attractor. Its frequency Ω as well as the spatial frequency K of the transverse modulation agrees well with the values predicted by stability analysis.

The transverse modulation of beam intensities I_1 and I_2 plotted as a function of time [Figs. 6(a) and 6(b)] displays a moving pattern. The transverse modulations seem to originate in the beam center, and left-going and right-going modulations run across the beam profile until
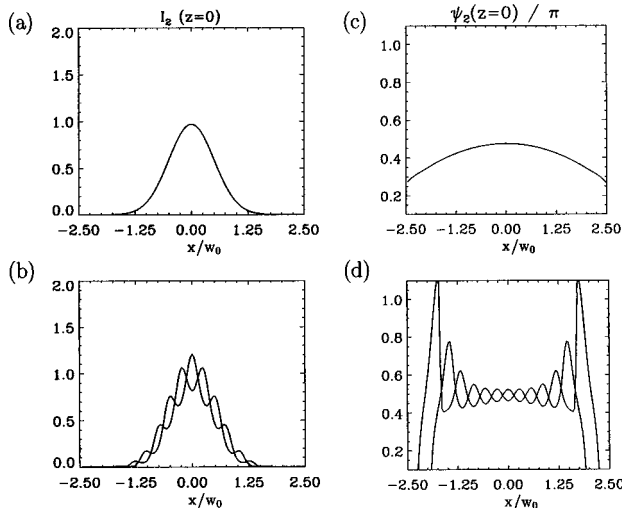

Fig. 5. Transverse intensity and phase profiles of beam A_2 when it leaves the crystal at $z = 0$: (a), (c) below threshold for $E_0 = -1.8E_d$; (b), (d) above threshold for $E_0 = -2.0E_d$ at times t and $t + T/2$.
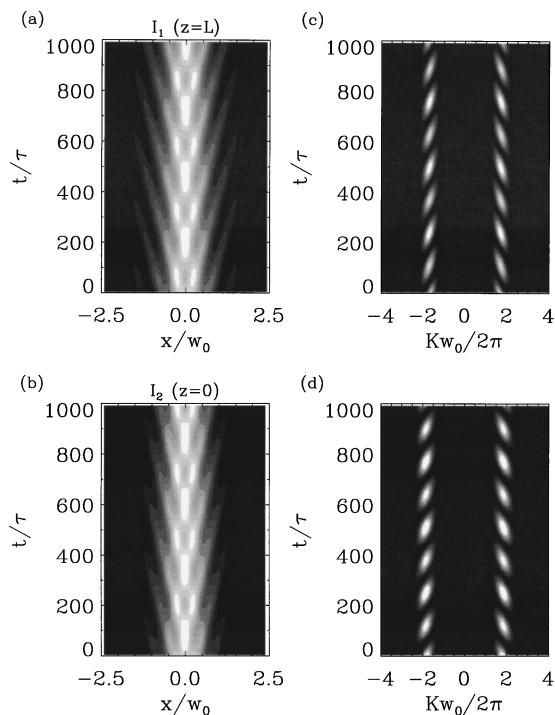

Fig. 6. Spatiotemporal dynamics above the instability threshold at $E_0 = -2.0E_d$. Running transverse waves in the near field for (a) I_1 and (b) I_2, and (c), (d) wandering spots in the far field; the pump beams have been subtracted. $\Gamma_0 L = 2.0$, $f = 0.025$, $r_0 = 20.09$, $\alpha L = 0$.

they disappear at the edges. Such spatiotemporal patterns are known as running transverse waves.[22] The nature of the running transverse waves is clarified in Subsection 4.C below by means of an eigenmode analysis. We observe only symmetric structures with respect to the beam center. Even for asymmetric initial conditions in the refractive-index grating the attractor is symmetric after the long transients have died away.

The running transverse wave pattern occurs in the optical near field. Here it possesses a characteristic spatial length scale given by the critical wavelength $\Lambda_c = 2\pi/K_c$ of $\sim 47~\mu$m in our case. This type of pattern is analogous to the well-known roll pattern in one transverse dimension. In the far field these transverse patterns appear as two wandering spots [Figs. 6(c) and 6(d)] under a characteristic angle $\theta_c \approx K_c/k_0$ of ~ 0.31 deg with respect to the direction of propagation. We have assumed the light of a He–Ne laser and a beam radius of $\sim 90~\mu$m. They emerge as a pair of faint spots, become brighter while they move inward, and finally fade away, and another pair already begins to emerge. These spots are the sideband beams that correspond to the transverse wave vectors $+K$ and $-K$. The perturbation amplitudes a_+, b_-, etc. of the linear analysis grow to the finite amplitudes of the spots in the nonlinear system.

A. Linear Absorption

Photorefractive crystals exhibit strong absorption of light. There are two types of absorption present. The coherent absorption of photons produces free charge carriers for the PR effect, and a photochromic absorption grating is formed.[23] Incoherent absorption phenomena are described by means of linear damping of the light fields, which we are considering here. In Fig. 7 we compare the threshold predicted by stability analysis with our numerical simulations. We find that the threshold is raised and the frequency of the limit cycle oscillation is lowered by linear absorption effective along the propagation direction. The spatial frequency of the transverse mode is predicted to increase with stronger absorption, but in the numerical simulations we find that it remains almost the same.

The oscillation frequency decreases more in the simulations than expected from linear stability analysis. In the numerical simulations we find a somewhat higher threshold, as we mentioned in Section 3. Therefore we look for a critical oscillation frequency of the most unstable transverse mode given by stability analysis for critical values of E_0 $\sim 10\%$ above the actual threshold. Here linear stability analysis still provides a good correction, indicated by the dashed curve in Fig. 7(b). So the temporal behavior is slowed when the onset of pattern formation is shifted to higher field strength. Above threshold the oscillation frequency increases with increasing strength of the external field (Fig. 8). The spatiotemporal structure of the running transverse wave, however, is not changed by linear absorption.

B. Focusing Effects

In Section 3 we discussed the influence of the polarity of the externally applied field on the stability behavior. We report here on an effect of focusing that is biased by the
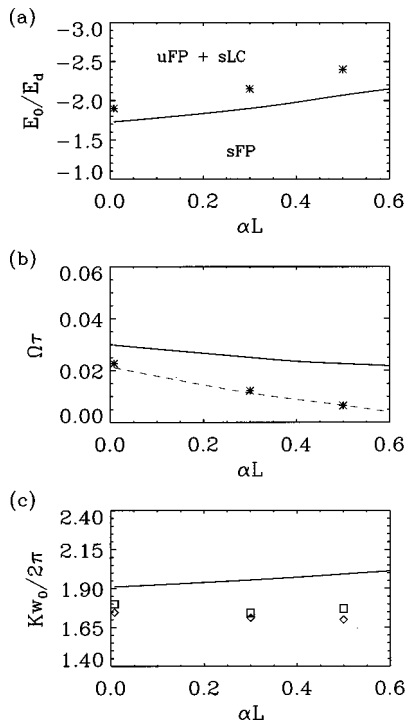
Fig. 7. (a) Bifurcation diagram of the primary instability threshold (solid curve) displaying the critical values of $E_0 < 0$ as a function of αL for fixed $\Gamma_0 L = 2.0$ and $r_0 = 20.09$. (b) Oscillation frequency, (c) spatial frequency. Asterisks, results obtained from numerical simulations. For the spatial frequency one obtains different values for I_1 ($\diamond$) and I_2 ($\square$). The dashed curve in (b) indicates the correction for the frequency given by stability analysis.
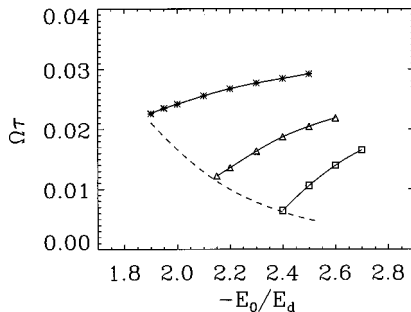

Fig. 8. Frequency behavior above threshold for different values of αL: ($\ast$) 0.0, ($\triangle$) 0.3, ($\square$) 0.5, obtained from numerical simulations. Solid curves, cubic splines through the data points; dashed curve, onset of pattern formation given by stability analysis.

transverse modulational instability in this wave mixing geometry. Above the instability threshold transverse modulations occur in the beam profile. If we now further increase the strength of the external field, the amplitudes of the modulation increase [Fig. 9(a)]. For I_1 two regions of high intensity appear at the edges of the beam profile, whereas the center of beam I_2 steepens noticeably [Fig. 9(c)].

Below threshold the slowly varying envelope of Q, and hence the change in the refractive index, is homogeneous in the transverse direction. When the threshold is crossed a transverse inhomogeneity in Q emerges, caused by the modulation of beam profiles. Slightly above threshold the transverse modulation of the grating ampli-

tude becomes visible [Fig. 10(a)]. The importance of this effect was realized by Honda and Banerjee[10] when they pointed out that one should not neglect the interference between each of the pumps and its own sideband beams in performing stability analysis. The bright stripe structure seen in the middle of the distribution is the source of the modulational structure in the refractive index, indicating the focusing–defocusing tendency of the beams. The additional structure seen in the wings of the distri-
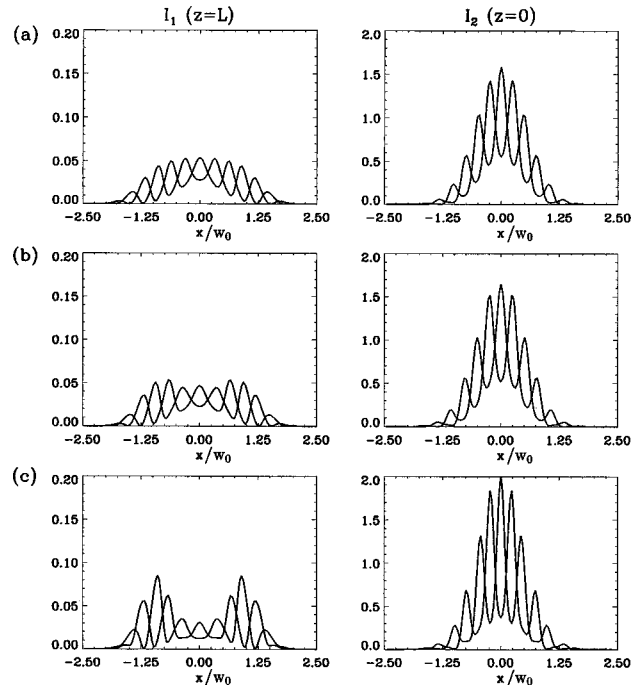

Fig. 9. Transverse intensity profiles for $E_0/E_d =$ (a) -2.2, (b) -2.3, (c) -2.6 at times t and $t + T/2$.
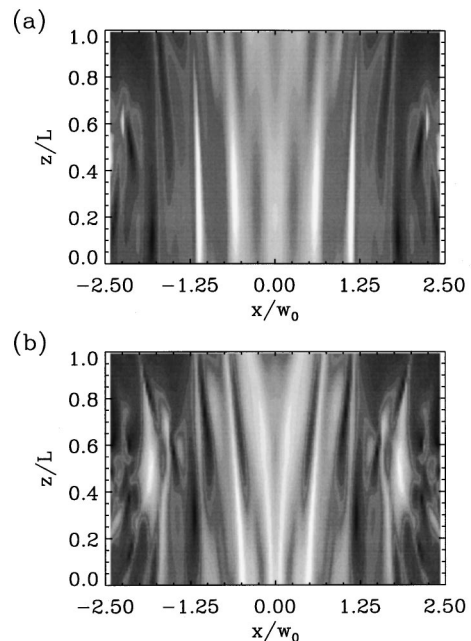

Fig. 10. Spatial distribution of the slowly varying envelope of $|Q|$ within the crystal at one instant of time for $E_0/E_d =$ (a) -2.0, (b) -2.6.

bution is caused by failure to take into account the dark intensity I_d. Adding I_d of the order of 10^{-4} to the total intensity in Eq. (2) will suppress these artificial bright spots. For a field strength of $E_0 = -2.6E_d$ a V-type structure in Q occurs [Fig. 10(b)] and exerts a strong influence on the wave mixing process in the crystal. The backward beam (I_2) focuses toward the beam center, whereas the forward beam (I_1) defocuses into the two sides of the V-shaped region.

The mechanism is the same as for all self-focusing processes; i.e., the beams become focused into regions of high refractive index. However, it is also different in the sense that it requires a transverse modulational instability to happen. This focusing effect is a dynamic process, because the index grating is a running grating and the spatial distribution of Q oscillates around the mean V-shaped structure.

C. Eigenmode Analysis

To characterize quantitatively the spatial structures and their dynamics, we apply a singular-value decomposition, also known as the Karhunen–Loève decomposition,[24,25] to the spatiotemporal patterns. Singular-value decomposition was originally developed for the task of pattern recognition but has generally proved to be a powerful tool for determining and distinguishing different spatiotemporal degrees of freedom, which are often hard to detect by visual inspection. By computing and analyzing the basic eigenmodes we obtain a better insight into the mechanisms that lead to complex spatiotemporal dynamics.

The time-varying part of the intensity pattern $\delta I(x, t) = I(x, t) - \langle I(x, t) \rangle_T$ is decomposed according to Karhunen and Loève into an orthogonal set of eigenmodes $p^{(i)}(x)$ and their time-dependent expansion coefficients $a^{(i)}(t)$:

$$\delta I(x, t) = \sum_i a^{(i)}(t) p^{(i)}(x). \qquad (15)$$

The eigenvalues $\lambda^{(i)}$ determine the probability of occurrence of the corresponding eigenvectors $p^{(i)}$ in the intensity pattern $I(x, t)$. Figure 11 displays the spectra of the normalized eigenvalues $\lambda^{(i)}$ for the intensity patterns of the running transverse waves slightly and far above threshold. The eigenvalues decrease rapidly with increasing mode index i. Higher eigenmodes become important for the pattern farther away from threshold. Note that, as far as the order of magnitude is concerned, the eigenvalues are arranged in pairs. The sum of the two largest eigenmodes contains more than 97% of the information of the original spatiotemporal structure, and higher eigenmodes simply contribute small corrections.

In Fig. 12 the transverse dependence of the two dominating eigenmodes, the time series of the expansion coefficients, and the resulting spatiotemporal substructures $\delta I^{(i)}(x, t)$ are shown. Such a substructure by itself represents a standing transverse wave [Figs. 12(a) and 12(d)]. The first eigenmode, $p^{(1)}$ [Fig. 12(b)], consists of a finite wave packet with a basic spatial frequency K_0, and its expansion coefficient [Fig. 12(c)] displays a temporal frequency Ω_0. The second eigenmode, $p^{(2)}$ [Fig. 12(e)], has a more complex spatial structure, though its expan-
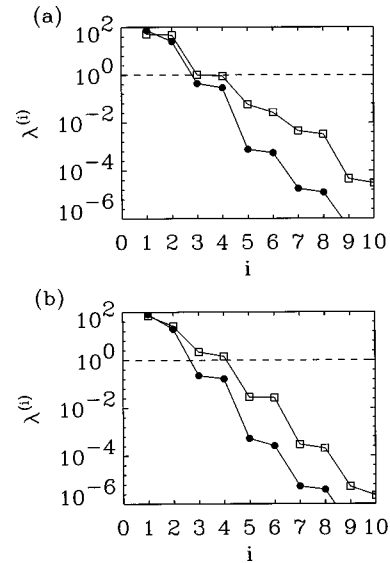

Fig. 11. Spectra of normalized eigenvalues $\lambda^{(i)}$ (in percent) for the intensity patterns of (a) I_1 and (b) I_2 with (●) $E_0/E_d = -2.0$ and (□) $E_0/E_d = -2.6$.
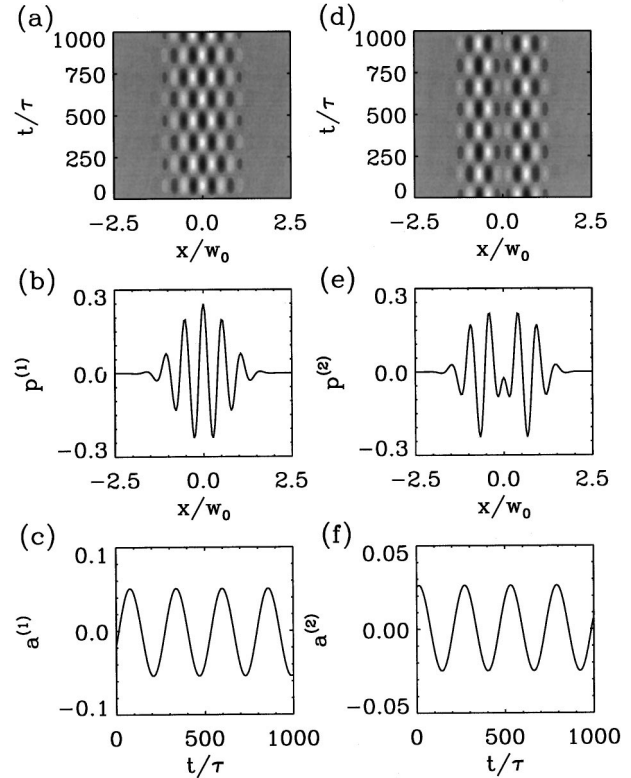

Fig. 12. (a), (d) Spatiotemporal substructures: the two dominating eigenmodes (b) with $\lambda^{(1)} \approx 80.22\%$ and (e) with $\lambda^{(2)} \approx 19.39\%$ and (c), (f) their time-dependent expansion coefficients of the running transverse wave of Fig. 6(b).

sion coefficient [Fig. 12(f)] possesses the same temporal frequency Ω_0. The Fourier spectra of the eigenmodes (Fig. 13) reveal that the second eigenmode contains two basic spatial frequencies, $K_1 = K_0 - \Delta K$ and $K_2 = K_0 + \Delta K$, that are separated by a frequency gap of $2\Delta K$ around K_0. As the eigenmodes are finite wave packets, the spectra themselves are broadened. The transverse

spatial structure and the temporal evolution of these two eigenmodes are shifted by $\pi/2$ relative to each other. This phase shift allows the two standing-wave patterns to combine into a running transverse wave.

K_0 agrees well with the critical frequency K_c predicted by linear stability analysis and thus represents the transverse modulation that is due to the spontaneous destabilization of the homogeneous fixed point. The occurrence of ΔK indicates a secondary bifurcation immediately after the primary bifurcation, which we presume originates from the finite transverse Gaussian beam profile. ΔK preserves the transverse symmetry with respect to the beam center and is related to the simultaneous occurrence of a right-going and a left-going transverse wave.

In Fig. 14 the basic spatial frequencies K_0 and ΔK are shown with respect to the bifurcation parameter E_0. Because of the dynamic focusing effects described in Subsection 4.B, K_0 and ΔK are smaller for I_1 than for I_2. They increase for I_2 and decrease for I_1 with increasing $|E_0|$, indicating that the dynamic focusing effects become stronger farther away from threshold. As a consequence the angle of the sideband beams of I_1 and the angle of the
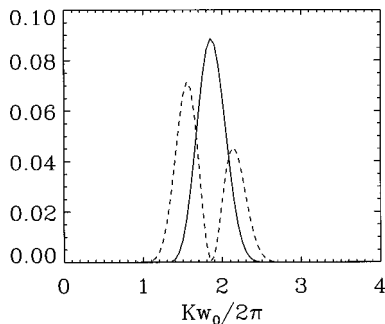

Fig. 13. Spatial Fourier spectra of the two largest eigenmodes from Fig. 12(b) (solid curve) and from Fig. 12(e) (dashed curve).
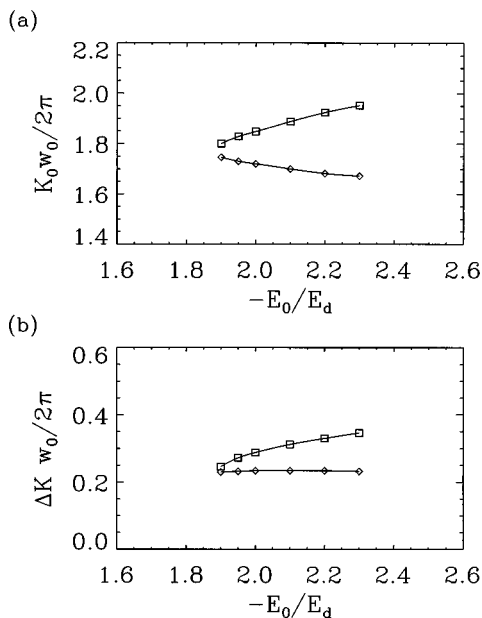

Fig. 14. Behavior of (a) the basic spatial frequency K_0 and (b) the frequency gap ΔK as functions of the applied field strength for ($\diamond$) beam I_1 and ($\square$) beam I_2. Solid curves, cubic splines through the data points.

sideband beams of I_2 are no longer equal. Because of the running grating they also have become time dependent, which leads to the behavior of the wandering spots in Figs. 6(c) and 6(d).

Extrapolation of K_0 and ΔK toward the threshold corroborates the statement that the secondary bifurcation happens immediately after the primary one, because K_0 and ΔK approach the same value for I_1 and I_2, and, in particular, ΔK obviously tends toward a nonzero value. The amplitudes of both eigenmodes, of course, go to zero at threshold.

A similar bifurcation behavior was already observed, e.g., in a two-level laser model with positive frequency detuning.[26] There it could be shown by means of an order parameter equation that above threshold both standing and running transverse wave patterns exist but that only the latter ones form a stable solution.

5. CONCLUSIONS

The counterpropagation of two laser beams in a sluggish photorefractive medium with nonlocal response has been investigated analytically and numerically. A nonautonomous linear stability analysis for arbitrary parameter values of the coupling strength and the pump ratio has been performed, predicting the onset of spontaneous destabilization of the homogeneous steady-state solution. Above the primary instability threshold in our numerical simulations we observed the occurrence of running transverse waves in the optical near field and wandering spots in the far field. Both the temporal frequency of the limit cycle oscillation and the spatial frequency of the transverse modulation agree well with the values predicted by the stability analysis. The effect of linear absorption shifts the onset of pattern formation to a higher field strength and results in slower oscillation frequencies of the patterns but does not change the type of running transverse wave. Above threshold, transverse modulations in the amplitude of the reflection grating cause dynamic focusing effects of the beams. An eigenmode analysis identifies the running transverse waves as secondary instabilities. Close to threshold, the running transverse waves are formed through the combination of two fundamental substructures. Only spatially symmetric patterns were found.

Numerical simulations performed here were done in one transverse dimension. We plan to extend the simulations to two transverse dimensions. Based on the one-dimensional results, we expect that different patterns will appear in the far field: two wandering spots, or a continuous ring, or moving spots on a ring forming squares or hexagons. Which of these structures will be seen will depend on boundary and geometrical conditions.

In performing stability analysis it has become clear that modulation depth of the steady-state fixed-point solutions is important for stability. Whenever the instability threshold is reached, the modulation depth is no longer small. This result leads to an inconsistency with the Kukhtarev model. Phenomenological correction functions introduced so far[27] were able to explain experimental gain measurements,[28] for example. However, the nonlinear response of the complex amplitude of the space-

charge field to a sinusoidal intensity grating results in a different dynamic behavior in the case of an externally applied static electric field[29] and also in complicated behavior of the phases.[30] In our opinion inclusion of these correction functions is not sufficient to adequately describe pattern formation for high modulation depths.

A further remark concerning the temporal evolution of patterns is in order. The applied field always induces dynamic instabilities through Hopf bifurcation because of the removal of frequency degeneracy. The Kukhtarev standard model, which has been employed to describe temporal evolution here and in all other publications studied, was applied under the assumption that the photorefractive time constant depends inversely on the total intensity. For the interaction through transmission gratings in the plane-wave limit the total intensity is constant. However, in the case of reflection gratings the total intensity has become z dependent. Owing to the Gaussian beam profile, it also has become x dependent. As a consequence, the time constant varies in different regions within the crystal. The crystal reacts faster in illuminated regions, and the building of refractive-index changes proceeds at different paces. This result has no influence on the steady state and does not qualitatively change our results close to the instability point. However, it affects the temporal evolution of spatiotemporal patterns and may alter the dynamic focusing, which is absent in the steady state. We plan to address these questions in the future.

ACKNOWLEDGMENTS

REFERENCES

1. W. J. Firth and C. Pare, "Transverse modulational instabilities for counterpropagating beams in Kerr media," Opt. Lett. **13**, 1096–1098 (1988).
2. W. J. Firth, A. Fitzgerald, and C. Pare, "Transverse instabilities due to counterpropagation in Kerr media," J. Opt. Soc. Am. B **7**, 1087–1097 (1990).
3. G. G. Luther and C. J. McKinstrie, "Transverse modulational instability of counterpropagating light waves," J. Opt. Soc. Am. B **9**, 1047–1060 (1992).
4. J. B. Geddes, R. A. Indik, J. V. Moloney, and W. J. Firth, "Hexagons and squares in a passive nonlinear optical system," Phys. Rev. A **50**, 3471–3485 (1994).
5. G. Grynberg, "Transverse-pattern formation for counterpropagating beams in rubidium vapor," Europhys. Lett. **18**, 689–695 (1992).
6. J. B. Geddes, J. V. Moloney, and R. Indik, "Spontaneous transverse spatial pattern formation due to Brillouin scattering of counterpropagating light fields," Opt. Commun. **90**, 117–122 (1992).
7. T. Honda, "Hexagonal pattern formation due to counterpropagation in $KNbO_3$," Opt. Lett. **18**, 598–600 (1993).
8. T. Honda, "Flow and controlled rotation of the spontaneous optical hexagon in $KNbO_3$," Opt. Lett. **20**, 851–853 (1995).
9. P. P. Banerjee, H.-L. Yu, D. A. Gregory, N. Kukhtarev, and H. J. Caulfeld, "Self-organization of scattering in photorefractive $KNbO_3$ into a reconfigurable hexagonal spot array," Opt. Lett. **20**, 10–12 (1995).
10. T. Honda and P. P. Banerjee, "Threshold for spontaneous pattern formation in reflection-grating-dominated photorefractive media with mirror feedback," Opt. Lett. **21**, 779–781 (1996).
11. B. Sturman and A. Chernykh, "Mechanism of transverse instability of counterpropagation in photorefractive media," J. Opt. Soc. Am. B **12**, 1384–1386 (1995).
12. A. I. Chernykh and B. I. Sturman, "Threshold for pattern formation in a medium with a local photorefractive response," J. Opt. Soc. Am. B **14**, 1754–1760 (1997).
13. M. Saffman, D. Montgomery, A. A. Zozulya, K. Kuroda, and D. Z. Anderson, "Transverse instability of counterpropagating waves in photorefractive media," Phys. Rev. A **48**, 3209–3215 (1993).
14. M. Saffman, A. A. Zozulya, and D. Z. Anderson, "Transverse instability of energy exchanging counterpropagating two-wave mixing," J. Opt. Soc. Am. B **11**, 1409–1417 (1994).
15. M. R. Belić, J. Leonardy, D. Timotijević, and F. Kaiser, "Transverse effects in double phase conjugation," Opt. Commun. **111**, 99–104 (1994).
16. M. R. Belić, J. Leonardy, D. Timotijević, and F. Kaiser, "Spatiotemporal effects in double phase conjugation," J. Opt. Soc. Am. B **12**, 1602–1616 (1995).
17. N. V. Kukhtarev, V. B. Markov, S. G. Odulov, M. S. Soskin, and V. L. Vinetskii, "Holographic storage in electrooptic crystals. I. Steady state," Ferroelectrics **22**, 949–960 (1979).
18. W. Krolikowski, M. R. Belić, M. Cronin-Golomb, and A. Bledowski, "Chaos in photorefractive four-wave mixing with a single grating and a single interaction region," J. Opt. Soc. Am. B **7**, 1204–1209 (1990).
19. P. Yeh, "Contra-directional two-wave mixing in photorefractive media," Opt. Commun. **45**, 323–326 (1983).
20. M. R. Belić, "Comment on using the shooting method to solve boundary-value problems involving coupled-wave equations," Opt. Quantum Electron. **16**, 551–557 (1984).
21. O. Sandfuchs, J. Leonardy, F. Kaiser, and M. R. Belić, "Transverse instabilities in photorefractive counterpropagating two-wave mixing," Opt. Lett. **22**, 498–500 (1997).
22. J. Leonardy, F. Kaiser, M. R. Belić, and O. Hess, "Running transverse waves in optical phase conjugation," Phys. Rev. A **53**, 4519–4527 (1996).
23. M. R. Belić, "Exact solution to photorefractive and photochromic two-wave mixing with arbitrary dependence on fringe modulation," Opt. Lett. **21**, 183–185 (1996).
24. M. Kirby, "Minimal dynamical systems from PDEs using Sobolev eigenfunctions," Physica D **57**, 466–475 (1992).
25. O. Hess and E. Schöll, "Eigenmodes of the dynamically coupled twin-stripe semiconductor lasers," Phys. Rev. A **50**, 787–792 (1994).
26. G. K. Harkness, W. J. Firth, J. B. Geddes, J. V. Moloney, and E. M. Wright, "Boundary effects in large-aspect-ratio lasers," Phys. Rev. A **50**, 4310–4317 (1994).
27. Ch. H. Kwak, S. Y. Park, J. S. Jeong, H. H. Suh, and E.-H. Lee, "An analytical solution for large modulation effects in photorefractive two-wave couplings," Opt. Commun. **105**, 353–358 (1994).
28. J. E. Millerd, E. M. Garmire, M. B. Klein, M. B. Klein, B. A. Wechsler, F. P. Strohkendl, and G. A. Brost, "Photorefractive response at high modulation depths in $Bi_{12}TiO_{20}$," J. Opt. Soc. Am. B **9**, 1449–1453 (1992).
29. G. A. Brost, "Numerical analysis of photorefractive grating formation dynamics at large modulation in BSO," Opt. Commun. **96**, 113–116 (1993).
30. L. B. Au and L. Solymar, "Higher harmonic gratings in photorefractive materials at large modulation with moving fringes," J. Opt. Soc. Am. A **7**, 1554–1561 (1990).